DOI:
10.1002/mrm.26198

Document Version
Peer reviewed version

Jacobian Weighted Temporal Total Variation for Motion Compensated Compressed Sensing Reconstruction of Dynamic MRI

Javier Royuela-del-Val[1], Lucilio Cordero-Grande[2], Federico Simmross-Wattenberg[1], Marcos Martín-Fernández[1] and Carlos Alberola-López[1]

[1]Laboratorio de Procesado de Imagen, Universidad de Valladolid, Valladolid, Spain.

[2]Centre for the Developing Brain, Division of Imaging Sciences and Biomedical Engineering, King's College London, London, UK.

Corresponding Author:

Javier Royuela-del-Val,

Laboratorio de Procesado de Imagen,

Universidad de Valladolid,

ETSI de Telecomunicación, Campus Miguel Delibes,

47011 Valladolid, Spain.

Email: jroyval@lpi.tel.uva.es

Phone: +34 983 423660, ext. 5590

Keywords: Dynamic MRI reconstruction; compressed sensing; groupwise registration; motion estimation

Grant sponsor: Spanish Ministerio de Ciencia e Innovación and the European Regional Development Fund (ERDF-FEDER), **Grant number:** TEC2014-57428-R.

Grant sponsor: Spanish Ministerio de Ciencia e Innovación, **Grant number:** TEC2013-44194-P.

Grant sponsor: Junta de Castilla y León, **Grant number:** VA-136U13.

Grant sponsor: Universidad de Valladolid and Banco de Santander FPI-UVa Fellowship Program.

Word count: 2788

Abstract

Purpose: To eliminate the need of spatial intra-frame regularization in a recently reported dynamic MRI compressed-sensing based reconstruction method with motion compensation and to increase its performance.

Theory and Methods: We propose a new regularization metric based on the introduction of a spatial weighting measure given by the Jacobian of the estimated deformations. It shows convenient discretization properties and, as a byproduct, it also provides a theoretical support to a result reported by others based on an intuitive design. The method has been applied to the reconstruction of both short and long axis views of the heart of four healthy volunteers. Quantitative image quality metrics as well as straightforward visual assessment are reported.

Results: Short and long axis reconstructions of cardiac cine MRI sequences have shown superior results than previously reported methods both in terms of quantitative metrics and of visual assessment. Fine details are better preserved due to the lack of additional intra-frame regularization, with no significant image artifacts even for an acceleration factor of 12.

Conclusions: The proposed Jacobian Weighted temporal Total Variation results in better reconstructions of highly undersampled cardiac cine MRI than previously proposed methods and sets a theoretical ground for forward and backward predictors used elsewhere.

Introduction

Temporal Total Variation (tTV) has provided good results in dynamic MRI reconstruction methods (1–3) based on the Compressed Sensing (CS) theory (4, 5). However, these methods remain sensitive to large inter frame motion usually present in dynamic MRI due to breathing, phase misalignments in, e.g., cardiac perfusion, or the natural motion of the heart in cine MRI. Since this motion reduces the sparsity of the signal, the achievable acceleration factor shrinks as well.

Several methods in the literature introduce some knowledge about motion to promote signal sparsity prior to the computation of the tTV; the underlying assumption is that motion can be described with fewer parameters than the changes it introduces in the dynamic sequence (6). In MASTeR (7), motion between each pair of consecutive frames in cardiac cine MRI is estimated from an initial reconstruction and used to predict adjacent frames. Residuals between the actual and predicted frames are assumed sparse. In order to prevent bias, motion is estimated both forwards (FW) and backwards (BW). In the deformation corrected (DC)-CS framework (8) the

dynamic sequence and the inter frame motion are jointly estimated and the overall procedure is applied to compensate for respiratory motion in cardiac perfusion imaging. In addition, the sparse domain can be chosen independently of the motion estimation procedure. In our previous works, GW-CS (9) and kt-WiSE (10), a related approach is presented. The motion estimation (ME) step is based on a B-spline deformation model and on a groupwise (GW) temporal registration algorithm; the procedure turns out to be robust to the artifacts introduced by the undersampled acquisition. However, as stated in (9), the motion compensation operator led to image artifacts in the reconstructed image. Therefore, a spatial regularization term was introduced to eliminate these artifacts at the cost of increasing, consequently, the complexity of the method.

In this paper, we propose a new sparse regularization term given by the inclusion of the Jacobian of the estimated non-rigid deformation in the DC-tTV. This regularization term, hereafter referred to as Jacobian Weighted tTV (JW-tTV), has a three fold advantage, namely: 1) avoids the presence of the reconstruction artifacts, eliminating the need of additional spatial regularization, 2) has convenient discretization properties that facilitate its implementation and 3) provides theoretical support for the FW and BW motion operators introduced empirically in MASTeR. The modified tTV has been applied to the reconstruction of cine sequences following the scheme in GW-CS.

Theory

Dynamic MRI Compressed Sensing Reconstruction

We represent the MRI sequence to be reconstructed m as a stack of N continuous 2D images $m_n(\boldsymbol{x})$, with spatial location $\boldsymbol{x} \in \mathcal{X} \subset \mathbb{R}^2$ and temporal index $n = 1, 2, \ldots, N$. Once noise decorrelation is applied, the acquired MRI data can be modeled as (11)

$$\mathbf{y}_{n,c} = \int_{\boldsymbol{x}\in\mathcal{X}} m_n(\boldsymbol{x}) S_c(\boldsymbol{x}) \exp\left(-i\mathbf{k}_n^T \boldsymbol{x}\right) \mathrm{d}\boldsymbol{x} + \mathbf{n}_{n,c} \qquad [1]$$

where $\mathbf{k}_n$ represents the set of k-space positions sampled at the indexed time n, $S_c(\boldsymbol{x})$ the sensitivity profile of each coil in parallel MRI and $\mathbf{n}_{n,c}$ a circularly symmetric white Gaussian noise. In vector form, Eq. [1] can be rewritten as

$$\mathbf{y} = \mathbf{E}(m) + \mathbf{n} \qquad [2]$$

where the operator $\mathbf{E}$ comprises the multiplication by coil sensitivities and the evaluation of the Fourier transform (FT) at the k-space positions $\mathbf{k}_n$ for $n = 1, 2, \ldots, N$.

Under the CS theory, the sequence m can be recovered from the undersampled data $\mathbf{y}$ by solving the following minimization problem (3)

$$\hat{m} = \arg\min_{m} \ \frac{1}{2}\|\mathbf{y} - \mathbf{E}(m)\|_{\ell_2}^2 + \lambda\|\Psi(m)\|_{\ell_1} \qquad [3]$$

where ℓ_1 regularization term promotes sparsity of the solution in the transformed domain given by Ψ. For cardiac cine MRI, tTV has been successfully applied and can be defined

$$\|\nabla_t(m)\|_{\ell_1} = \frac{1}{|\mathcal{X}|N} \int_{\boldsymbol{x}\in\mathcal{X}} \sum_{n=1}^{N} |m_{n+1}(\boldsymbol{x}) - m_n(\boldsymbol{x})| \ \mathrm{d}\boldsymbol{x} \qquad [4]$$

where cyclical motion has been considered by setting $m_{N+1}(\boldsymbol{x}) = m_1(\boldsymbol{x})$.

Jacobian Weighted tTV with Motion Compensation

In order to compensate for the inter frame motion, we introduce a motion compensation operator $\mathcal{T}_{\boldsymbol{\Theta}}$ that deforms each of the cardiac phases to a common, average, motion state (8, 9). The transform is governed by the set of parameters Θ. The resulting reference configuration can be regarded as a material point coordinate system. However, as discussed in (9), its direct application may lead to severe artifacts in the regions of the reconstructed images where large deformations are involved.

Moreover, when the tTV is computed after the application of $\mathcal{T}_{\boldsymbol{\Theta}}$, the accumulated differences are implicitly weighted according to their corresponding areas in the motion corrected sequence $\mathcal{T}_{\boldsymbol{\Theta}}(m)$, as opposed to those in the one to be reconstructed; this is illustrated in Figure 1a, where a diagram shows the change in area induced by the spatial deformation and how it relates to its Jacobian[1]. Intuitively, when the transformation gives rise to a contraction —Jacobian lower than 1—, it will be over-regularized during reconstruction, since it occupies a larger area in the reference configuration. Contrarily, enlarged areas —Jacobian higher than 1— will be under-regularized. Figure 1b shows an example of the spatial distribution of the Jacobian at systole on real data. In Supporting Video 1, the example is reproduced for the whole cardiac cycle.

Consequently, we propose to counteract this effect by locally weighting each temporal difference according to its corresponding area in the original sequence. We define a JW-tTV regularization

[1]Notice that although $\mathcal{T}_{\boldsymbol{\Theta}}(m)$ stands for the motion corrected sequence, transformations are actually defined in the opposite direction, i.e., from material coordinates to spatial coordinates.

term given by[2]:

$$\|m\|_{\mathcal{T}_\Theta} = \frac{1}{|\mathcal{X}|N} \int_{\boldsymbol{x}\in\mathcal{X}} \sum_{n=1}^{N} |m_{n+1}(\mathbf{T}_{n+1}(\boldsymbol{x})) - m_n(\mathbf{T}_n(\boldsymbol{x}))|\, \mathcal{J}_{\mathbf{T}_{n+1/2}}(\boldsymbol{x})\, \mathrm{d}\boldsymbol{x} \quad [5]$$

where $\boldsymbol{u}_n = \mathbf{T}_n(\boldsymbol{x})$ stands for the spatial deformation that maps each material point $\boldsymbol{x}$ in the motion compensated sequence to its corresponding spatial location $\boldsymbol{u}_n$ at instant n. Given the discrete nature of index n, the transformation Jacobian at $n+1/2$ is approximated by

$$\mathcal{J}_{\mathbf{T}_{n+1/2}}(\boldsymbol{x}) \approx \frac{1}{2}\left[\mathcal{J}_{\mathbf{T}_n}(\boldsymbol{x}) + \mathcal{J}_{\mathbf{T}_{n+1}}(\boldsymbol{x})\right] \quad [6]$$

what allows us, after permuting summation and integration orders, to split Eq. [5]:

$$\begin{aligned}\|m\|_{\mathcal{T}_\Theta} \propto \sum_{n=1}^{N} \Bigg\{ & \int_{\boldsymbol{x}\in\mathcal{X}} |m_{n+1}(\mathbf{T}_{n+1}(\boldsymbol{x})) - m_n(\mathbf{T}_n(\boldsymbol{x}))|\, \mathcal{J}_{\mathbf{T}_n}(\boldsymbol{x})\, \mathrm{d}\boldsymbol{x} + \\ & \int_{\boldsymbol{x}\in\mathcal{X}} |m_{n+1}(\mathbf{T}_{n+1}(\boldsymbol{x})) - m_n(\mathbf{T}_n(\boldsymbol{x}))|\, \mathcal{J}_{\mathbf{T}_{n+1}}(\boldsymbol{x})\, \mathrm{d}\boldsymbol{x} \Bigg\}\end{aligned} \quad [7]$$

By means of the changes of variable $\mathbf{T}_n(\boldsymbol{x}) = \boldsymbol{u}_n \rightarrow \mathcal{J}_{\mathbf{T}_n}(\boldsymbol{x})\mathrm{d}\boldsymbol{x} = \mathrm{d}\boldsymbol{u}_n$ and $\mathbf{T}_{n+1}(\boldsymbol{x}) = \boldsymbol{u}_{n+1} \rightarrow \mathcal{J}_{\mathbf{T}_{n+1}}(\boldsymbol{x})\mathrm{d}\boldsymbol{x} = \mathrm{d}\boldsymbol{u}_{n+1}$ we write:

$$\begin{aligned}\|m\|_{\mathcal{T}_\Theta} \propto \sum_{n=1}^{N} \Bigg\{ & \int_{\boldsymbol{u}_n\in\mathcal{X}} |m_{n+1}(\mathbf{T}_{n+1,n}(\boldsymbol{u}_n)) - m_n(\boldsymbol{u}_n)|\, \mathrm{d}\boldsymbol{u}_n + \\ & \int_{\boldsymbol{u}_{n+1}\in\mathcal{X}} |m_{n+1}(\boldsymbol{u}_{n+1}) - m_n(\mathbf{T}_{n,n+1}(\boldsymbol{u}_{n+1}))|\, \mathrm{d}\boldsymbol{u}_{n+1} \Bigg\}\end{aligned} \quad [8]$$

where we have defined $\mathbf{T}_{i,j} = \mathbf{T}_i \circ \mathbf{T}_j^{-1}$ —details on how to obtain $\mathbf{T}_j^{-1}$ are provided in the Appendix—. That is, $\mathbf{T}_{i,j}$ deforms m_i to m_j (12). In Eq. [8] we return from the common material point coordinate system to the local spatial system of each frame while retaining the motion information from $\mathcal{T}_\Theta$. Defining $B_i(m_i) = m_i \circ \mathbf{T}_{i,i-1}$ and $F_i(m_i) = m_i \circ \mathbf{T}_{i,i+1}$,

$$\|m\|_{\mathcal{T}_\Theta} \propto \sum_{n=1}^{N} \int_{\boldsymbol{u}\in\mathcal{X}} \|B_{n+1}(m_{n+1}) - m_n\|_{\ell_1} + \|F_n(m_n) - m_{n+1}\|_{\ell_1} \mathrm{d}\boldsymbol{u} \quad [9]$$

where B_i and F_i are two motion operators that map each frame i onto its previous (BW) and following (FW) frames, respectively. In Eq. [9] the dependence of the integrand with $\boldsymbol{u}$ is omitted for notational simplicity.

[2]We consider that motion is entirely located within the image boundaries so integration domains do not effectively change with the change of variables.

It is worth mentioning that Eq. [9] resembles the regularization term used in MASTeR (7). With our result we provide theoretical support for the use of both BW and FW motion operators empirically introduced in that work. Moreover, while in MASTeR these operators arise directly from the sequential ME technique applied, in our proposal they are obtained from $\mathcal{T}_\Theta$ regardless of the ME technique used. This enables us to apply a GW temporal registration scheme which has shown more robustness to undersampling artifacts than sequential methods (9). Figure 1c summarizes the differences between the proposed method, the original GW-CS and MASTeR.

Methods

The objective function on which GW-CS is grounded is (9)

$$\hat{m} = \arg\min_{m} \frac{1}{2}\|\mathbf{y} - \mathbf{E}(m)\|_{\ell_2}^2 + \lambda_t \|\nabla_t(\mathcal{T}_\Theta(m))\|_{\ell_1} + \lambda_s \|\Psi(m)\|_{\ell_1} \quad [10]$$

with Ψ a spatial wavelet transform. In this paper, the ℓ_1 terms are substituted by the JW-tTV term (Eq. 8); the last term, which is the spatial regularization term, is dropped. The JW-tTV reconstruction is then formulated as

$$\hat{m} = \arg\min_{m} \frac{1}{2}\|\mathbf{y} - \mathbf{E}(m)\|_{\ell_2}^2 + \lambda \|m\|_{\mathcal{T}_\Theta} \,. \quad [11]$$

A scheme of the proposed algorithm follows:

Implementation description of JW-tTV based reconstruction of undersampled dynamic MRI.

input:

$\mathbf{y}$: undersampled k-t data

$\mathbf{E}$: encoding operator

λ: sparsity regularization parameter

initialization:

$k \leftarrow 0$

$m^0 \leftarrow$ Eq. [3]; initial CS reconstruction.

while $k < k_{max}$. number of iterations **do**

$\Theta^{k+1} \leftarrow$ GW temporal registration. See (9) for details.

$m^{k+1} \leftarrow$ CS reconstruction. Solve Eq. [11] for Θ^{k+1}. (For comparison, at this step the original GW-CS algorithm solves Eq. [10]).

$k \leftarrow k + 1$

end

output: $\hat{m} = m^{k_{max}}$

In the implementation m is discretized in a regular Cartesian grid and interpolation is used to compute $\mathcal{T}_\Theta(m)$. In our experiments, a bicubic interpolation provided better reconstructions than the bilinear scheme used in (9) without a noticeable increment in computational cost. The whole reconstruction algorithm was implemented in MATLAB (MathWorks, Natick, MA) and the optimization problems in Equations [3] and [9] were solved with the NESTA algorithm (13) on a PC with two Intel XEON E5-2695 v3 @ 2.30GHz with 14 cores and 64 GB of RAM.

The parameter λ was fitted to achieve the highest SER —defined later— in a region around the heart for one of the datasets for an acceleration factor of 8 and kept constant for the rest. The same approach was followed to fit λ_t and λ_s in GW-CS. The obtained values are $\lambda = 0.01$, $\lambda_t = 0.003$ and $\lambda_s = 0.0003$. For the experiments in Figure 4a (see below), in which the proposed method is complemented with a spatial regularization term at the only purpose of comparison, its weight is set to 0.001 (with the original λ kept constant).

Two quantitative error metrics were used for reconstruction comparison. Firstly, the signal-to-error ratio (SER), defined as

$$\mathrm{SER(dB)} = 20 \log_{10} \frac{\|m\|_{\ell_2}}{\|m - \hat{m}\|_{\ell_2}},$$

where m denotes the fully sampled image and $\hat{m}$ the image reconstructed from undersampled data. Second, the structural similarity index —SSIM— (14) was also used as a complementary quantitative metric.

In vivo experiments

Short axis (SA) and long axis (LA) views of the heart were obtained from four healthy volunteers on a 3T Philips Achieva equipment with a 32-element cardiac coil. Other relevant scan parameters include: b-SSFP sequence, TR/TE/flip angle = 3.3 ms/1.57 ms/45°, FOV = 320×320 mm^2 and slice thickness = 8 mm. 30 cardiac phases were reconstructed with retrospective ECG synchronization. Fully sampled images were converted back to k-t space and considered as single coil acquisitions. Data was retrospectively undersampled with an inhomogeneous sampling pattern following a Gaussian distribution along the phase encoding direction simulating different acceleration factors ranging from 2 to 12.

Results

Figure 2 shows the reconstruction of a midventricular SA slice with the four methods compared —regular CS reconstruction with tTV, MASTeR, original GW-CS and JW-tTV—. Temporal profiles, corresponding frames at systole and error images are shown. Figure 3 shows the equivalent results obtained for a left two-chambers view of the same dataset.

Methods with motion compensation outperform regular CS for high acceleration factors. However, MASTeR shows a faster degradation of the image quality that is more evident in the temporal profiles in Figures 2b and 3b, where the edges of the myocardial are severely distorted and some erratic motion can be observed —white arrows—. This effect, clearly appreciable in Supporting Videos 2 and 3, is due to the sequential ME technique applied, which turns out to be affected by the strong undersampling artifacts present in the initial reconstruction. As for GW-CS, we can see how dynamic behavior is better preserved given the more robust ME technique. However, in Figures 2c and 3c, structure edges become more blurred for high acceleration factors due to the spatial regularization introduced. Still; however, some residual high frequency artifacts remain for the highest acceleration factor. With JW-tTV there is no need of such a spatial regularization and myocardium edges as well as papillary muscles are better preserved. In the LA views, the mitral valve can be appraised both in MASTeR and the JW-tTV reconstructions for an acceleration factor

of 8; however, in GW-CS the spatial regularization hinders the retrieval of such a small structure from the undersampled data —white arrows—.

In order to analyze the effects of the proposed JW-tTV and the spatial regularization separately, in Figure 4a one SA view has been reconstructed with both the original GW-CS method and with JW-tTV with and without a spatial regularization term based on the complex wavelet transform (CWT). The GW-CS reconstruction without spatial regularization shows high frequency artifacts, specially at end-diastole and systole, which are removed with spatial regularization; however, edge sharpness is strongly affected and thin details are lost. In the proposed method, the additional spatial regularization does not involve an appreciable improvement in image quality but affects complexity and computational cost of the algorithm. The sensitivity of the algorithm to different initializations is analyzed in Figure 4b. Three different sequences where used as initial guesses; namely, the ground truth images from the fully sampled data, an initial CS reconstruction with tTV and an initial CS reconstruction spatially over-regularized with CWT. Both the visual appearance and quantitative metrics shown are very similar in the three cases, with slight superior scores for the fully sampled initialization. These results suggest that the method is robust against large differences in the initialization and, as it iterates, it is able to recover from poor initial guesses.

In Figure 5 plots of the SER and SSIM obtained for the reconstructions of the four SA datasets are represented. Both GW-CS and JW-tTV outperform MASTeR reconstructions in terms of SER and SSIM and differences increase with the acceleration factor. However, there is no appreciable difference between the GW-CS and JW-tTV in terms of these quantitative metrics. We understand that achieving comparable performance with one less control parameter and with better edge definition is worth taking.

Discussion and Conclusions

In this work we have proposed a modification of the tTV metric commonly used in the CS reconstruction of dynamic MRI sequences by means of a weighting factor given by the Jacobian of the transformation $\mathcal{T}_\Theta$ that maps the position of each point in the motion compensated sequence to its corresponding position in the original sequence. At first sight, this could be regarded as an adaptive TV related to the one proposed in (15), where spatial TV regularization is leveraged in the presence of spatial edges to preserve sharpness. However, in our proposal we intend to account for the effect of the relative size of each region in the image, regardless of the underlying structures.

With this modification, the resulting tTV metric resembles the regularization term proposed in MASTeR (7). However, in this case theoretical support has been given to the inclusion of both FW and BW motion compensation terms and the definition of these terms has been made independent of the ME technique. This has allowed us to apply the robust GW temporal registration approach previously proposed in GW-CS (9) so differences with respect to MASTeR are maintained; with the JW-tTV modification proposed in this paper, there is no need of the additional spatial regularization introduced in GW-CS —the term weighted by λ_s in Eq. [10]—, a fact of great importance since now sharper edges and small details in the images, even for acceleration factors as high as 12, are maintained. The erratic motion observed in MASTeR reconstructions for high acceleration factors —see Supporting Video 2 for factor 8 and beyond— reveals how the final reconstruction may be corrupted by ME errors, which occasionally could be misinterpreted as false cardiac function abnormalities. This fact makes even clearer the need of a robust ME technique as we understand ours is. In any case, the impact of motion artifacts should be further studied to validate the clinical utility of these methods at such high acceleration factors.

As indicated in Eq. [8], the transform $\mathcal{T}_\Theta$ that results from the estimated motion should be invertible. Proper spacing of the B-splines control points and the introduction of a regularization term (see the Appendix) encourages its invertibility. Even though this property is not strictly guaranteed, the experiments realized so far have always led to invertible transforms.

The presented experiments have been performed simulating an undersampled acquisition in Cartesian trajectories. Execution times at the different acceleration factors and orientations considered and for the four volunteers datasets ranged 8–10 min for MASTeR reconstruction, 15–22 min for GW-CS and 11–18 min for JW-tTV. Generally speaking, higher acceleration factors led to faster reconstructions given the lesser data involved. The higher execution times of GW-CS and JW-tTV with respect to MASTeR are mainly due to the GW registration; an additional advantage of JW-tTV is the lower execution time due to the elimination of the spatial regularization term. Needless to say, these methods could benefit from more efficient implementations in compiled languages and its execution on GPU devices.

This registration method can be easily extended to other image modalities where the assumption of constant pixel intensity does not hold —as in contrast enhanced MRI— by proper election of the similarity metric (16). Moreover, the advanced normalization tools (ANTs) package (17) provides versatile diffeomorphic registration methods in which the invertibility of the deformation is guaranteed. The adaptation of these methods to our application will be studied. As for the

sparsity term, in this situation the introduction of the Jacobian weighting is not directly applicable to common sparse representations such as the temporal Fourier transform. However, higher order temporal differences could be used in Eq. [5] to enforce smooth evolution of single pixel intensities while preserving from staircase effects. This approach has shown to be very effective when applied in the spatial domain (18) and will be further explored.

Appendix

Inversion of the deformation field

In order to define the operator $\mathbf{T}_{i,j}$, the inverse transformation $\mathbf{T}_j^{-1}$ is needed. Since the inverse of a B-spline cannot be analytically obtained, a numerical optimization approach is adopted. In general, $\mathbf{T}_j^{-1}$ will not be a B-spline transform. Therefore we directly look for the set of material points $\boldsymbol{x}_n$ that, when mapped by $\mathbf{T}_n$, result in the regular Cartesian grid of spatial locations in which the original images are discretized —see implementation description—. To this end, for each n we solve

$$\boldsymbol{x}_n^* = \arg\min_{\boldsymbol{x}} \sum_{\boldsymbol{u}_n \in \mathcal{X}'} \|\mathbf{T}_n(\boldsymbol{x}) - \boldsymbol{u}_n\|_{\ell_2}^2 \qquad [12]$$

with $\mathcal{X}'$ the set of discrete pixels in $\mathcal{X}$, using nonlinear conjugate gradient optimization. Solving Eq. [12] is equivalent to storing an approximation of the evaluation of $\mathbf{T}_n^{-1}$ for every $\boldsymbol{u}_n \in \mathcal{X}'$. We approximate $\mathbf{T}_{i,j}(\boldsymbol{u}_j) \mid_{\boldsymbol{u}_j \in \mathcal{X}'} = \mathbf{T}_i(\mathbf{T}_j^{-1}(\boldsymbol{u}_j)) \mid_{\boldsymbol{u}_j \in \mathcal{X}'} \approx \mathbf{T}_i(\boldsymbol{x}_j^*)$. The previous approach has the advantage that no deformation model assumption for $\mathbf{T}_n^{-1}$ is needed. On the other side, it is only valid for the set of points in $\mathcal{X}'$ for which Eq. [12] is solved, which is compatible with the reconstruction method at hand.

In the registration algorithm, even though the invertibility of $\mathbf{T}_n$ is not guaranteed, it is enforced by proper selection of the spacing between B-spline deformation control points and the regularization of the deformation fields with a term related to the elastic energy of the transformation (19) —see (9) for details—. In our experiments, control point spacing was 4 mm along both spatial dimensions. The weight given to the regularization term was tuned to minimize the residual motion —measured as the tTV— when the deformations estimated from an initial CS reconstruction at an acceleration factor of 8 were applied to the corresponding fully sampled sequence. This way, the registration method is made robust against residual undersampling artifacts and prevented from becoming non-invertible, while keeping it flexible enough to describe cardiac motion.

References

1. Adluru G, McGann C, Speier P, Kholmovski EG, Shaaban A, DiBella EV. Acquisition and reconstruction of undersampled radial data for myocardial perfusion magnetic resonance imaging. J Magn Reson Imag 2009;29:466–473.

2. Feng L, Srichai MB, Lim RP, Harrison A, King W, Adluru G, Dibella EVR, Sodickson DK, Otazo R, Kim D. Highly accelerated real-time cardiac cine MRI using k–t SPARSE-SENSE. Magn Reson Med 2013;70:64–74.

3. Feng L, Grimm R, Tobias Block K, Chandarana H, Kim S, Xu J, Axel L, Sodickson DK, Otazo R. Golden-angle radial sparse parallel MRI: Combination of compressed sensing, parallel imaging, and golden-angle radial sampling for fast and flexible dynamic volumetric MRI. Magn Reson Med 2014;72:707–717.

4. Donoho DL. Compressed sensing. IEEE Trans Inf Theory 2006;52:1289–1306.

5. Candès EJ, Romberg J, Tao T. Robust uncertainty principles: Exact signal reconstruction from highly incomplete frequency information. IEEE Trans Inf Theory 2006;52:489–509.

6. Prieto C, Batchelor PG, Hill DLG, Hajnal JV, Guarini M, Irarrazaval P. Reconstruction of undersampled dynamic images by modeling the motion of object elements. Magn Reson Med 2007;57:939–949.

7. Asif MS, Hamilton L, Brummer M, Romberg J. Motion-adaptive spatio-temporal regularization for accelerated dynamic MRI. Magn Reson Med 2013;70:800–812.

8. Lingala SG, DiBella E, Jacob M. Deformation corrected compressed sensing (DC-CS): a novel framework for accelerated dynamic MRI. IEEE Trans Med Imag 2014;pp. 1–23.

9. Royuela-del Val J, Cordero-grande L, Martín-Fernández M, Simmross-Wattenberg F, Alberola-López C. Non-Rigid Groupwise Registration for Motion Estimation and Compensation in Compressed Sensing Reconstruction of Breath-Hold Cardiac Cine MRI. Magn Reson Med 2015; doi: 10.1002/mrm.25733.

10. Royuela-del Val J, Usman M, Cordero-Grande L, Simmross-Wattenberg F, Martín-Fernández M, Prieto C, Alberola-López C. Single Breath Hold Whole Heart Cine MRI With Iterative

Groupwise Cardiac Motion Compensation and Sparse Regularization (kt-WiSE). In Proceedings of the 23rd Annual Meeting of ISMRM. Toronto, CA 2015; p. 572.

11. Pruessmann KP, Weiger M, Scheidegger MB, Boesiger P. SENSE: Sensitivity encoding for fast MRI. Magn Reson Med 1999;42:952–962.

12. Metz CT, Klein S, Schaap M, van Walsum T, Niessen WJ. Nonrigid registration of dynamic medical imaging data using nD + t B-splines and a groupwise optimization approach. Med Image Anal 2011;15:238–249.

13. Becker S, Bobin J, Candès EJ. NESTA: A Fast and Accurate First-Order Method for Sparse Recovery. SIAM J Imaging Sci 2011;4:1–39.

14. Wang Z, Bovik AC, Sheikh HR, Simoncelli EP. Image quality assessment: From error visibility to structural similarity. IEEE Trans Imag Proc 2004;13:600–612.

15. Kamesh Iyer S, Tasdizen T, Dibella EVR. Edge-enhanced spatiotemporal constrained reconstruction of undersampled dynamic contrast-enhanced radial MRI. Magn Reson Imag 2012; 30:610–619.

16. Cordero-Grande L, Merino-Caviedes S, Aja-Fernández S, Alberola-López C, Alberola-lo C. Groupwise Elastic Registration by a New Sparsity-Promoting Metric: Application to the Alignment of Cardiac Magnetic Resonance Perfusion Images. IEEE Trans Pattern Anal Mach Intell 2013;35:2638–2650.

17. Avants BB, Tustison NJ, Song G, Cook PA, Klein A, Gee JC. A reproducible evaluation of ANTs similarity metric performance in brain image registration. NeuroImage 2011;54:2033–2044.

18. Knoll F, Bredies K, Pock T, Stollberger R. Second order total generalized variation (TGV) for MRI. Magn Reson Med 2011;65:480–491.

19. Rueckert D, Sonoda LI, Hayes C, Hill DLG, Leach MO, Hawkes DJ. Nonrigid registration using free-form deformations: application to breast MR images. IEEE Trans Med Imag 1999; 18:712–721.

Figures captions

Figure 1: a) Diagram of a SA view of the heart and the spatial deformations that map the reference configuration in material point coordinate system (bottom) to the systolic (top left) cardiac phase. At systole, the blood pool (lined regions) contracts, so the Jacobian of the deformation takes values lower than the unit in that region. On the contrary, the cardiac muscle thickens (shadowed regions) in the 2D view, so the Jacobian is greater than one in the myocardium. At diastole (top right), the situation is reversed. b) Example on real data at systole (top) and in the reference configuration (bottom left). Dashed circles delineate the myocardium. At bottom right, the spatial distribution of the Jacobian (bottom right) agrees with a). c) Table summarizing the main differences between MASTER, GW-CS and the proposed method. Analytically our sparse regularization term turns out to coincide with the one used by MASTER; however, we prefer to use the name JW-tTV to emphasize its origin.

Figure 2: Reconstructions of a short axis view of the heart. (a) Fully sampled systole phase with square ROI around the heart (top), detail of the ROI (bottom left) and temporal profile of a single slice along the indicated vertical line (bottom right). (b) Temporal profiles of the reconstructions with regular tTV regularization without motion compensation, MASTeR, the original GW-CS and the proposed method for the indicated acceleration factors ranging from 2 to 12. Difference images with respect to the fully sampled image appear next to each profile, multiplied by a scale factor of 5. (c) Reconstructed short axis views as in (b). White arrows indicate some erratic motion present in MASTeR reconstructions for high acceleration factors.

Figure 3: Reconstructions of a left two chambers view of the heart, presented following the same scheme as that in Figure 2. (a) Fully sampled systole phase with square ROI, detail of the ROI (bottom left) and temporal profile of a single slice (bottom right). (b) Temporal profiles and error images (scale factor of 5) of the reconstructions with the four compared methods for the indicated acceleration factors. (c) Reconstructed LA views as in (b). White arrows indicate the position of the mitral valve.

Figure 4: (a) Effects of the spatial regularization in a short axis view reconstruction. Systolic phase and temporal evolution of a horizontal line across left and right ventricles are shown. (b) Effect of different initializations (fully sampled, tTV and CWT) on the proposed algorithm. SER (dB) and SSIM index in the region of interest are shown below each final reconstruction. An acceleration factor of 10 was used.

Figure 5: SER(dB) and SSIM index calculated over a ROI around the heart in the SA views for the four volunteers with the proposed metric, original GW-CS and MASTeR.

Supporting Video 1: Motion estimation and compensation on a fully sampled short axis view of the heart. From left to right and top to bottom: original sequence, original sequence with the estimated deformation plotted in red, motion compensated sequence and spatial distribution of the Jacobian of the deformation along the cardiac cycle.

Supporting Video 2: Reconstruction of a short axis view of the heart with a regular CS reconstruction method with tTV, MASTeR, the original GW-CS method and the proposed JW-tTV for acceleration factors 2, 4, 8 and 12.

Supporting Video 3: Reconstruction of a long axis view of the heart with a regular CS reconstruction method with tTV, MASTeR, the original GW-CS method and the proposed JW-tTV for acceleration factors 2, 4, 8 and 12.

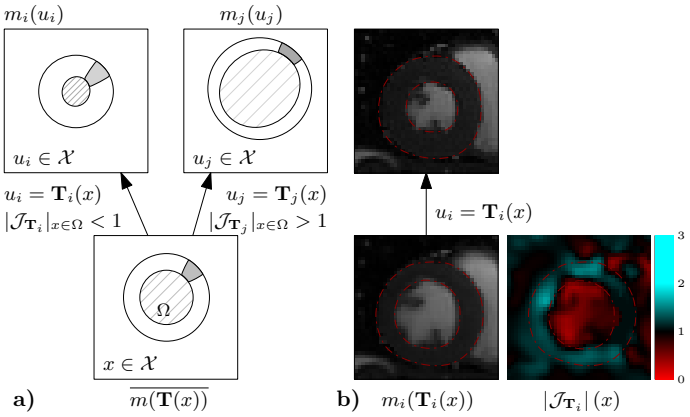

	Motion Estimation	Sparse Regularization
MASTER	Pairwise sequential, Forward/Backward	Sequential DC-tTV, Forward/Backward
GW-CS	Groupwise	Groupwise DC-tTV + Spatial regularization
Proposed	Groupwise	JW-tTV

c)

Figure 1: a) Diagram of a SA view of the heart and the spatial deformations that map the reference configuration in material point coordinate system (bottom) to the systolic (top left) cardiac phase. At systole, the blood pool (lined regions) contracts, so the Jacobian of the deformation takes values lower than the unit in that region. On the contrary, the cardiac muscle thickens (shadowed regions) in the 2D view, so the Jacobian is greater than one in the myocardium. At diastole (top right), the situation is reversed. b) Example on real data at systole (top) and in the reference configuration (bottom left). Dashed circles delineate the myocardium. At bottom right, the spatial distribution of the Jacobian (bottom right) agrees with a). c) Table summarizing the main differences between MASTER, GW-CS and the proposed method. Analytically our sparse regularization term turns out to coincide with the one used by MASTER; however, we prefer to use the name JW-tTV to emphasize its origin.

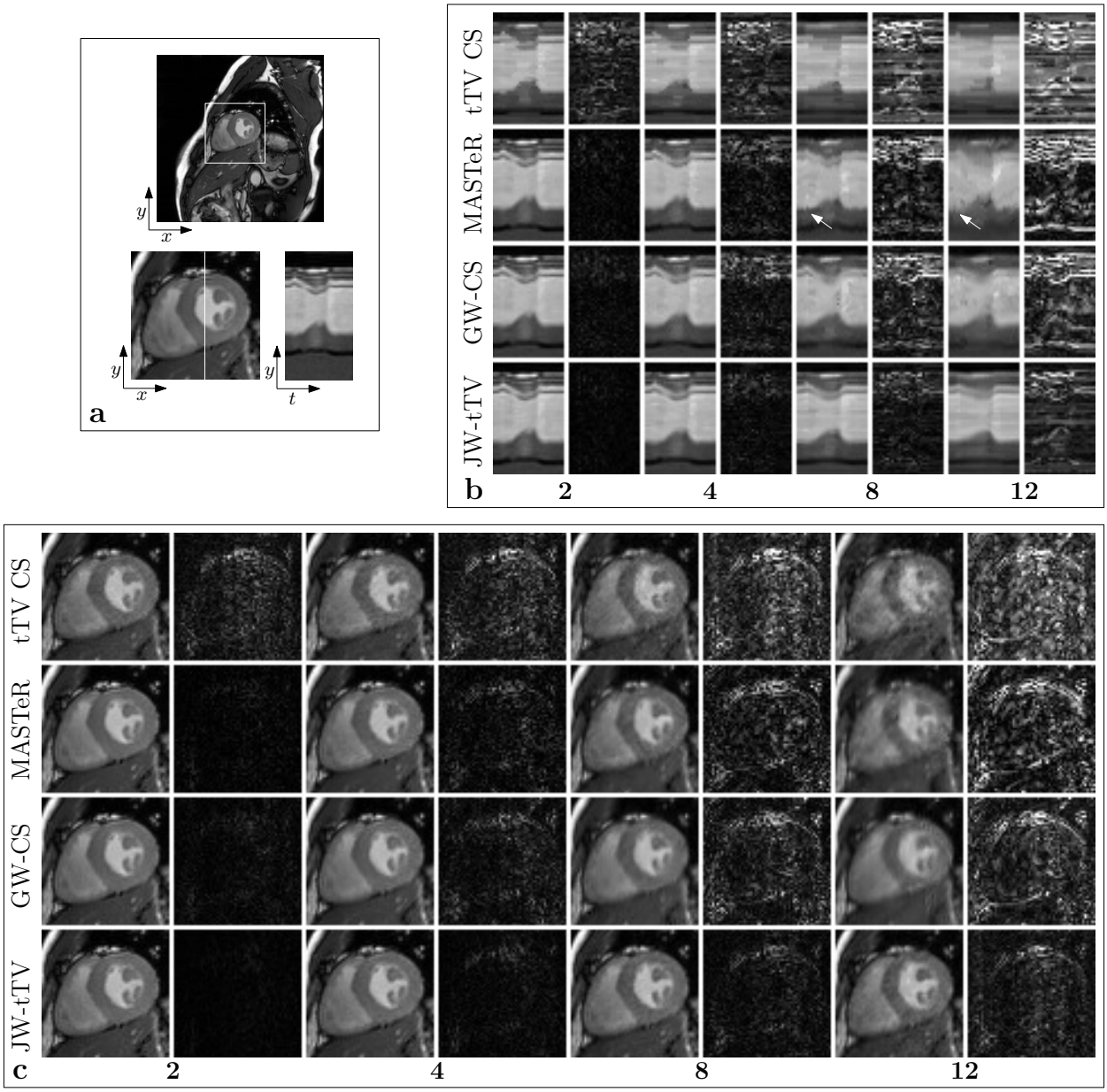

Figure 2: Reconstructions of a short axis view of the heart. (a) Fully sampled systole phase with square ROI around the heart (top), detail of the ROI (bottom left) and temporal profile of a single slice along the indicated vertical line (bottom right). (b) Temporal profiles of the reconstructions with regular tTV regularization without motion compensation, MASTeR, the original GW-CS and the proposed method for the indicated acceleration factors ranging from 2 to 12. Difference images with respect to the fully sampled image appear next to each profile, multiplied by a scale factor of 5. (c) Reconstructed short axis views as in (b). White arrows indicate some erratic motion present in MASTeR reconstructions for high acceleration factors.

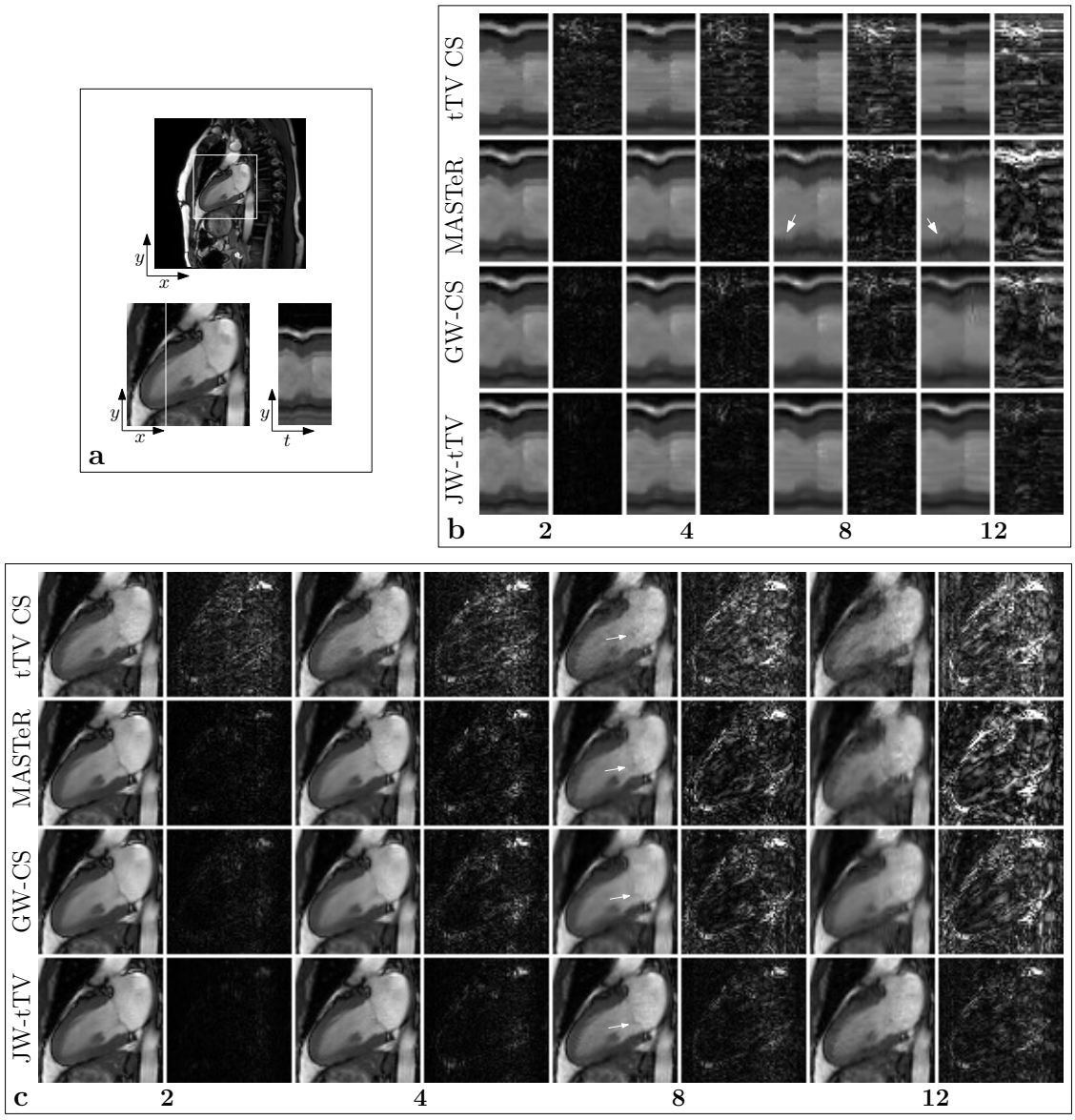

Figure 3: Reconstructions of a left two chambers view of the heart, presented following the same scheme as that in Figure 2. (a) Fully sampled systole phase with square ROI, detail of the ROI (bottom left) and temporal profile of a single slice (bottom right). (b) Temporal profiles and error images (scale factor of 5) of the reconstructions with the four compared methods for the indicated acceleration factors. (c) Reconstructed LA views as in (b). White arrows indicate the position of the mitral valve.

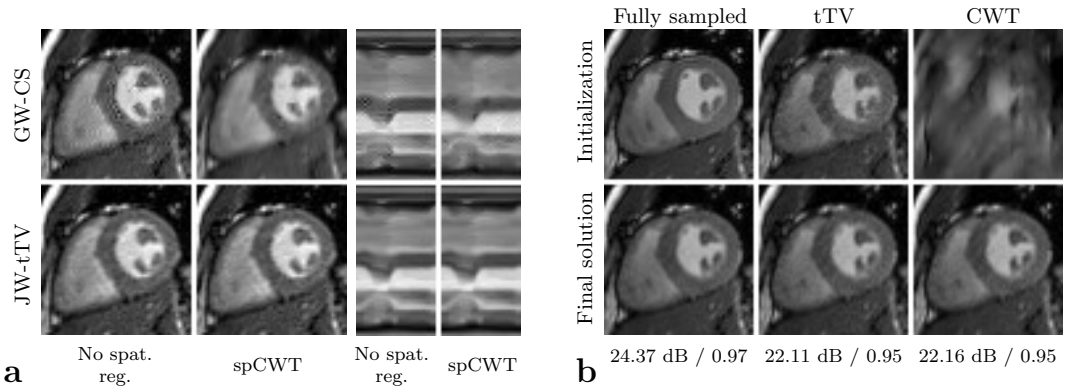

Figure 4: (a) Effects of the spatial regularization in a short axis view reconstruction. Systolic phase and temporal evolution of a horizontal line across left and right ventricles are shown. (b) Effect of different initializations (fully sampled, tTV and CWT) on the proposed algorithm. SER (dB) and SSIM index in the region of interest are shown below each final reconstruction. An acceleration factor of 10 was used.

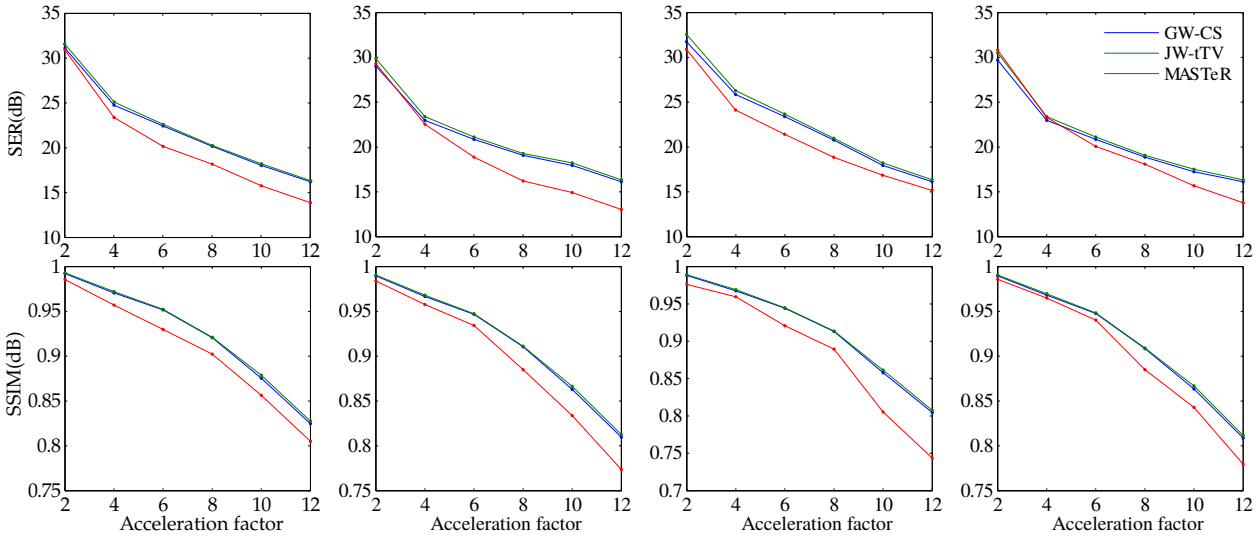

Figure 5: SER(dB) and SSIM index calculated over a ROI around the heart in the SA views for the four volunteers with the proposed metric, original GW-CS and MASTeR.